Author version

Published as:

Anderson, R. M., Ning, A., Xiang, R., van Schie, S. P. C., Sperry, M., Sarojini, D., Kamensky, D., & Hwang, J. T. (2023). Aerostructural predictions combining FEniCS and a viscous vortex particle method FLOWVPM. In AIAA SciTech 2023 Forum.
https://lsdolab.github.io/lsdo-publications/publication/anderson2023aerostructural/

BibTeX for this reference:

https://lsdolab.github.io/lsdo-publications/publication/anderson2023aerostructural/

```
@inproceedings{anderson2023aerostructural,
  author = {Ryan M. Anderson and Andrew Ning and Ru Xiang and Sebastiaan P. C. van Schie
    and Mark Sperry and Darshan Sarojini and David Kamensky and John T. Hwang},
  title = {Aerostructural Predictions Combining FEniCS and a Viscous Vortex Particle
    Method FLOWVPM},
  booktitle = {AIAA SciTech 2023 Forum},
  year = {2023}
}
```

Aerostructural Predictions Combining FEniCS and a Viscous Vortex Particle Method FLOWVPM

Ryan M. Anderson* and Andrew Ning†
Brigham Young University, Provo, UT 84602

Ru Xiang ‡, Sebastiaan P. C. van Schie §, Mark Sperry ¶, Darshan Sarojini ‖, David Kamensky **, John T. Hwang ††
University of California San Diego, 9500 Gilman Dr, La Jolla, CA 92093

Electric Vertical Takeoff and Landing (eVTOL) aircraft experience complex, unsteady aerodynamic interactions between rotors, wings, and fuselage that can make design difficult. We introduce a new framework for predicting aerostructural interactions. Specifically, we demonstrate the coupling of a finite element solver with Reissner-Mindlin shell theory for computing deflections and a viscous vortex particle for capturing wakes. We perform convergence studies of the aerodynamics and the coupled aerostructural model. Finally, we share some preliminary results of the dynamic aeroelastic response of Uber's eCRM-002 main wing, and share some qualitative observations.

I. Introduction

Multi-disciplinary design optimization (MDO) offers a powerful tool for design of next generation aircraft. Current MDO methods use numerical optimization method to allow practitioners to virtually design highly-coupled multidisciplinary engineering systems with hundreds of design variables and constraints.

A key multidisciplinary analysis involved in the design of aircraft is the coupling between aerodynamics, propulsion, and structures. This is a unsteady problem that can be very difficult to solve. In electric vertical takeoff and landing (eVTOL) aircraft, for example, the unsteady aerodynamic interactions between rotors, wings, and fuselage is difficult to predict. The effect of structural flexibility is significant when obtaining dynamic loads on aircraft wings [1]. For aircraft with distributed electric propulsion (DEP), the unsteady wake interactions affect the performance of rotors, wings [2, 3], and fuselage. In DEP, several electrically-driven propellers blow over wings, resulting in augmented lift and decreased drag due to favorable interactions between propellers and wings [4]. Rotors enjoy higher propulsive efficiency because the wing in the downwash acts like a stator for the propeller wake [5]. DEP may also improve stall behavior by increasing chordwise flow at high angles of attack [6]. DEP may help to reduce noise because many smaller propellers replace fewer, larger, louder ones [7]. For tilt-wing aircraft such as the V-22 Osprey that has two large propellers in front of the wing, and transitions between hover and forward flight; the unsteady nature of the rotor wake significantly influences the wing loading. Rotors blowing over wings have been shown to experience oscillating thrust, and increased torque [8]. Interestingly, the wing has little effect on the rotor [9]. These examples highlight the importance of using an unsteady model for both aerodynamic and structural considerations.

An analysis capability that captures unsteady aero-propulsive-structural interactions can be used to design novel aircraft in a design optimization framework. This enables sizing of the lifting surface, rotors, and the internal structure of the lifting surface. Design optimization of aircraft accounting for such interactions has been performed in the literature, where efficient one-way coupling of rotor-on-wing interactions using blade element momentum and lifting line models are used [10, 11]. However, these and other fast models require semi-empirical tuning parameters for accurate predictions [12], making conceptual level design a tenuous endeavor. Lifting line rotors with a panel method wing have also been used to capture propeller-wing interactions [13], as have actuator disk rotors with vortex sheet wake and wing surfaces [14]. Nonlinear beam models have been developed in the literature to size aircraft wings subjected

*Doctoral Candidate, Mechanical Engineering, AIAA Student Member
†Associate Professor, Mechanical Engineering, AIAA Associate Fellow
‡Ph.D. Student, Department of Mechanical and Aerospace Engineering, AIAA student member
§Ph.D. Student, Department of Mechanical and Aerospace Engineering, AIAA student member
¶Ph.D. Student, Department of Mechanical and Aerospace Engineering, AIAA student member
‖Postdoctoral Scholar, Department of Mechanical and Aerospace Engineering, AIAA member
**Assistant Professor, Department of Mechanical and Aerospace Engineering, AIAA member
††Assistant Professor, Department of Mechanical and Aerospace Engineering, AIAA member

to dynamic loads [15]. Beam models have been shown to give a good tradeoff between efficiency and accuracy [16]. However, the aerodynamic loads were obtained from steady vortex lattice method (VLM) codes. Mesh-based RANS [9] and LES [17] simulations have also been used, though these are generally more expensive.

The Viscous Vortex Particle Method (VPM) is an ideal tool for capturing these interactions, and offers significant speed-ups over mesh-based methods. It experiences less numerical dissipation than traditional mesh-based methods, and is very computationally efficient when vorticity is concentrated in a small portion of the flow, as in the wake of a rotor. It can be combined easily with fast, simple lift models like a vortex lattice or lifting line to obtain aerodynamic forces. Lee and Lee modeled rotational augmentation on a wind turbine using a nonlinear vortex lattice method, correcting the stall-blind vortex lattice method with 2-D lift coefficients to capture stall effects and convecting a vortex particle wake. Their results compared favorably with RANS simulations [18]. Alvarez and Ning predicted the performance of side-by-side rotors [19]. Montagnani et al. modeled a tilt-wing eVTOL aircraft with vortex particle wing and rotor wakes in conjunction with lifting line wings, source/doublet sheet fuselage, and blade element momentum rotors [3]. Savino et al. coupled classical potential flow models, vortex particles wakes, and a structural solver to predict the dynamic aeroelastic response of wings and rotors in unsteady situations [20].

Structural analysis and sizing for aircraft applications usually represent the structure as a shell model, which have a large number of design variables such as thicknesses, composite ply orientations, etc. Shell models are well-suited to handle the geometric and material nonlinearities in aircraft structures. Structural sizing can be efficiently performed using gradient-based optimization that relies on the adjoint method to efficiently compute the gradients [21] and hence decrease the computational cost associated with the numerical procedure. However, dynamic simulations with a shell model that have large Degrees of Freedom (DoF) is computationally intractable for many-query applications such as optimization. Hence, approaches mostly focus on the use of the adjoint method in shell model structural sizing by converting the dynamic loads into a set of critical *static* loads.

In this work, we present a tool to predict aerostructural dynamics using a shell model structural solver, non-linear lifting lines for lifting surfaces, and a viscous vortex particle method for wakes. The coupling between the solvers is handled by a novel solver-independent state representation to facilitate the transfer of state information [22]. We model the main wing of Uber's eCRM-002 eVTOL concept, available on NASA's OpenVSP database*, adopting the rotor geometry and cruise flight conditions suggested by Ha[23]. We demonstrate the difference in aerodynamic wing loading with and without the structural solver, as well as the aeroelastic oscillatory behavior with and without rotors.

II. Methods

The method combines a FEniCS-based [24] finite element solver with Reissner-Mindlin shell formulation to predict structural deflections, and a viscous vortex particle method to predict wake development using the open source code FLOWVPM and FLOWUnsteady†. The interface between aerodynamics and structural solvers is through a unified aeroelastic coupling formulation that conserves force & energy and allows for derivative computations in both steady-state and dynamic simulations [22].

A. Aerodynamics

Aerodynamics are modeled using FLOWUnsteady[25]. Rotors are modeled using an actuator line approach. Precalculated airfoil lift and drag lookup tables are provided for each cross section of the rotor. The Viterna method is used to extrapolate airfoil polars beyond stall. At each time step, the wake- and wing-induced velocities are applied to the lifting line representing the rotor, resulting in an effective angle of attack. Lookup tables are used to deduce the lift and drag of each rotor section. Finally, vortex particles that preserve the same circulation are placed on the actuator line, and are used to compute forces on the rotor using Jowkouski's theorem. These particles are convected from the trailing edge of the rotor to compose the wake.

Wings are modeled using a modified lifting line approach. Vortex horseshoes resembling a vortex lattice are placed along the wing, with the bound vortex aligned with the quarter-chord and trailing vortices extending to the trailing edge. The freestream, rotor-induced, and wake-induced velocities are computed at control points at the three-quarter-chord location, and vortex strengths are calculated to satisfy flow tangency using a linear solve. Aerodynamic forces are predicted using Jowkouski's theorem. Wakes are modeled using the VPM by convecting particles at the trailing edge of each horseshoe, with circulation strength equal to that of the corresponding vortex. When evolving the wake,

*https://hangar.openvsp.org/vspfiles/524
†https://github.com/byuflowlab/FLOWUnsteady

wing horseshoes are temporarily converted into vortex particles of equivalent circulation, and used to predict the wing-on-wake influence.

The wake itself is modeled using FLOWVPM[‡] [26], which is a reformulated vortex particle method, modified to conserve angular momentum, resulting in very numerically stable simulations. Pedrizzetti's relaxation scheme[27] is applied each timestep to ensure that the discretized vorticity field is divergence-free.

As FLOWUnsteady is written in the Julia language, we wrap it in Python using the package PyJulia[§] for integration with the structural solver.

B. Structures

The structural model uses shell elements to discretize the geometry of wing. A Python-based mesh generation tool is built for creating and dynamically updating the shell meshes corresponding to the changes of geometric variables in each design iteration.

The structural solver is based on a locking-free Reissner-Mindlin shell formulation [28] and implemented using the Python interface of FEniCS, which is an open-source finite element solver with automated derivative computation. Here we use second order continuous Lagrange interpolation for displacements and first order for rotations to prevent shear locking, with six DoFs in total per node. The aerodynamic loads are applied on the structural model as distributed loads on each vertices, and then the deformation results will be used for geometry updates in the aerodynamic model. This is where the two-way coupling happens.

A static structural analysis on the NASA Common Research Model (CRM) is used for validating the accuracy of the structural solver through comparison with Nastran. The wing root is clamped with all degrees of freedom there equal to zero, and a -1.0 g distributed load for gravity is applied on the wingbox structure (Figure 1). The results by FEniCS and Nastran agree with each other for both tip displacements and total strain energy, with a deviation less than 1.7% for all of the tests with different mesh refinements. Figure 2 shows the convergence study with refined meshes generated by Ansys ICEM, where both solvers converge to the same reference solution - the tip displacement result by Nastran with one inch element size.

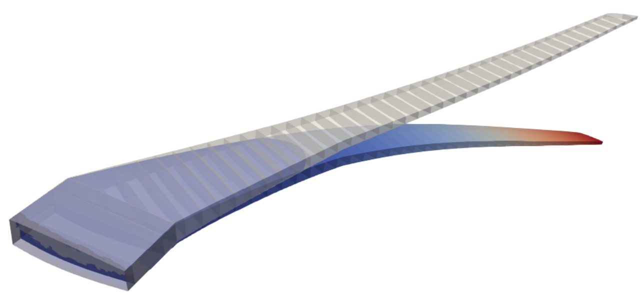

Fig. 1 Deflected wingbox of the Common Research Model under -1.0 g distributed load and clamped wing root boundary condition. Displacements are scaled by a factor of 10 for visualization. The undeflected wingbox model is illustrated in translucent gray.

For dynamic structural analysis, we use implicit midpoint rule (IMR) as the time stepping method, which is currently implemented in FEniCS for the simplicity of testing purposes and integrating the structural solver with other disciplines.

The structural solver can be easily integrated with CSDL by projecting the nodal evaluations of their problem inputs, such as thicknesses, external forces and material properties, onto the function spaces in FEniCS; and extracting the results, such as nodal displacements, as NumPy arrays to be used in the aerodynamic model or other post processors. It can also provide automated derivative computation for the partial derivatives of the PDE residual with respect to the design variables to enable gradient-based optimization problem.

[‡]https://github.com/byuflowlab/FLOWVPM.jl

[§]https://pyjulia.readthedocs.io/en/latest/

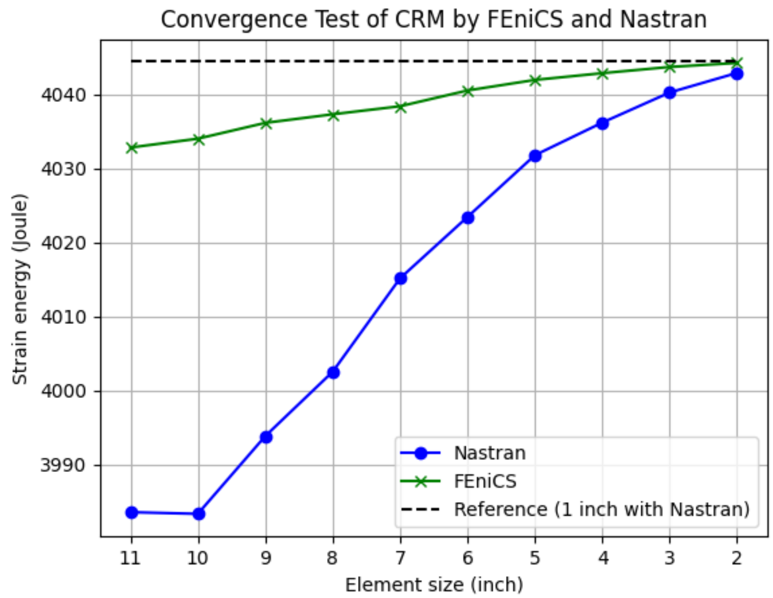

Fig. 2 Convergence study of total strain energy with respect to element size calculated in FEniCS and Nastran.

C. Coupling

We use a partitioned solver-independent approach to solve the coupled aeroelastic system. This approach follows the structure shown in Fig. 3: It allows for defining a solver-independent state representation to which the fluid and solid solvers are linked. Displacement and force mapping pairs $(T_{\boldsymbol{u},s}, T_{\boldsymbol{F},s})$, $(T_{\boldsymbol{u},a}, T_{\boldsymbol{F},a})$ are defined separately for the solid and fluid simulation models respectively. In this work no separate solver-independent state representation is used, and thus only one displacement and force mapping pair $(T_{\boldsymbol{u}}, T_{\boldsymbol{F}})$ is present. As is covered in [22], conservation of aeroelastic energy requires the maps of a mapping pair to satisfy a transpose relationship. We can thus define either $T_{\boldsymbol{u}}$ or $T_{\boldsymbol{F}}$, from which the other follows through the aforementioned transpose relationship. The resulting mapping pair conserves aeroelastic energy. We elect to define the displacement map $T_{\boldsymbol{u}}$, which converts the solid displacements $\boldsymbol{u}_s$ to displacements $\boldsymbol{u}_a$ of the aerodynamic geometry through $\boldsymbol{u}_a = T_{\boldsymbol{u}}\boldsymbol{u}_s$. This map is defined as composition of two projections. We first note that the solid deformation $\boldsymbol{u}_s$ is expressed in a quadratic function basis. In the first projection of $T_{\boldsymbol{u}}$ we interpolate $\boldsymbol{u}_s$ to the linear function basis on the solid mesh. There is a one-to-one correspondence between the solid mesh vertices and linear basis functions that we can then leverage to define the second projection.

Inverse distance weighting is then used with a Radial Basis Function to determine the displacement correlations between vertices of the solid and aerodynamic meshes. Each correlation is additionally weighted by the size of the support of the corresponding solid basis function. Lastly the correlations are normalized with the summed correlations for each aerodynamic mesh vertex. This defines the second of the projection steps that make up $T_{\boldsymbol{u}}$. Force map $T_{\boldsymbol{F}}$ follows directly through the aforementioned transpose property and conserves each individual force component. Interested readers are referred to [22] for a more in-depth treatment of the aeroelastic coupling approach that is used here.

III. Test Case and Results

A. Test Case Description: eCRM-002 Wing

The electric common research model (eCRM)-002 is a eVTOL concept released by Uber Elevate for on-demand aviation[¶]. It has six sets of propellers for vertical flight located on booms and the fuselage, and one tip mounted engine on each wing for forward flight. Figure 4 shows the eCRM-002 concept.

[¶]https://evtol.news/uber-elevate-ecrm-002/

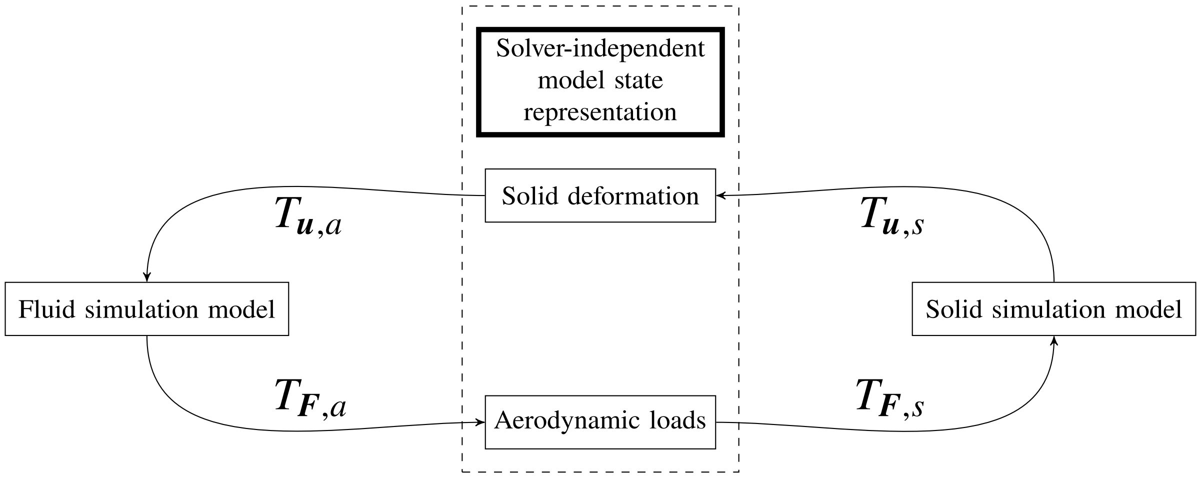

Fig. 3 Solver-independent coupling framework

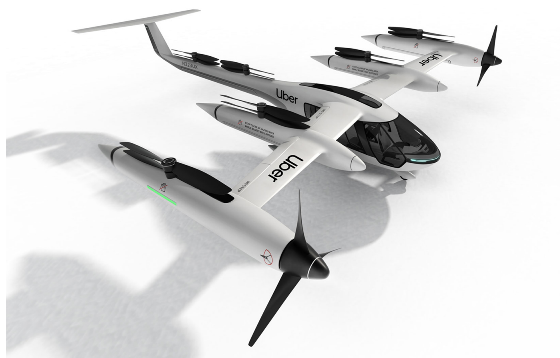

Fig. 4 The Uber Elevate eCRM-002 concept. Image from Electric VTOL News

In this work, we consider the forward-swept wings and the tip mounted propellers for the aeroelastic analysis. This test case is an ideal demonstrator of the capabilities developed in this work for several reasons:

1) The wingtip rotors are designed to ameliorate the wingtip vortices and thereby increase its aerodynamic efficiency. The VPM is especially efficient when vorticity is concentrated in a small portion of the flow, and therefore apt for capturing this interaction.
2) The propeller-wing interaction results in unsteady aerodynamic loads that are difficult to predict using legacy methods. The VPM is a fully unsteady solver with a LES turbulence model, making it ideal for capturing these interactions in an efficient manner.
3) The eCRM-002 has a cruise speed of 150 mph (241 km/hr), and, thus falls under the incompressible flow regime. VPM assumes incompressible flow within the wake, making the eCRM-002 a suitable test case.

Geometric details of the eCRM-002 are obtained from the publicly available OpenVSP[‖], with rotor details obtained from [23]. Table 1 gives the geometric details of the wing.

It is worth noting that these are preliminary results only, and meant to demonstrate successful coupling of the solvers more than to provide completely converged numerical data. For example, no spatial convergence test was performed on the structural mesh, and the solvers are converged just enough to show trends. However, we believe our results provide insight into aerostructural phenomena regarding eVTOL as well as the modeling technique itself.

[‖] https://hangar.openvsp.org/vspfiles/524

Table 1 eCRM-002 wing geometric specifications

Parameter	Value	Unit
S_{wing}	11.69	m^2
b_{wing}	10.64	m
c_{wing}	0.910	m
AR_{wing}	9.68	
θ_{root}	0	deg
θ_{tip}	1	deg
Γ_{wing}	−9	deg
ϕ_{wing}	6	deg

B. Convergence

First, convergence tests were performed with the aerodynamic solver only. In Figs. 5-6, we determine a timestep of $\Delta t = 0.001$ seconds with $n = 20$ wing control points to be sufficiently converged. Then, the structural solver was added and the timestep refined seeking convergence. Preliminary results of the convergence test are shown in Fig. **??**. Although the coupled solvers have not converged, we select a timestep of $\Delta t = 0.0005$ for now.

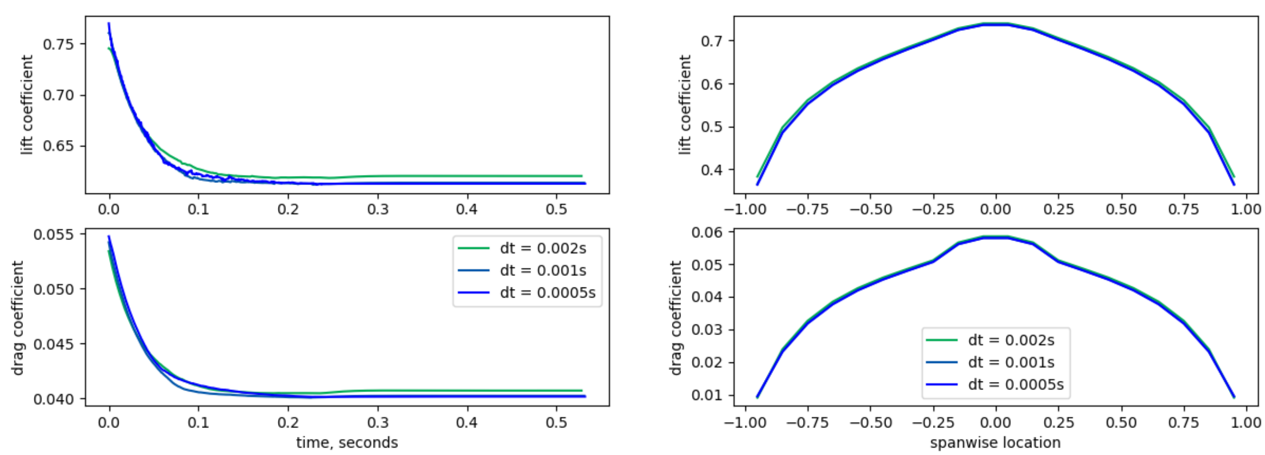

Fig. 5 Timestep convergence testing without rotors determines a timestep of $\Delta t = 0.001$ seconds.

Now we add rotors. Preliminary aerodynamics-only convergence testing is shown in Figs. 8-9. Note the oscillations in the lift coefficient vs. time due to the rotor.

C. Qualitative Wake Comparison with and without Structures

Although our preliminary results preclude converged data with rotors, we show qualitative trends noticed in the wake visualization. In Fig. 10, we observe the vortex particle wake behind the eCRM-002 formed without the structural solver for $n = 20$, $nr = 20$, and $\Delta t = 0.001$. In Fig. 11, we show the wake with the structural solver. In both cases, we note the vortex core at the center of the rotor wake, coincident with the wingtip vortex. However, in the case with the structural solver, the wingtip vortex is significantly more concentrated, while the aero-only case has its vorticity spread diffused throughout the rotor wake. It is possible that aeroelastic oscillations contribute to a stronger wingtip vortex compared to a rigid wing.

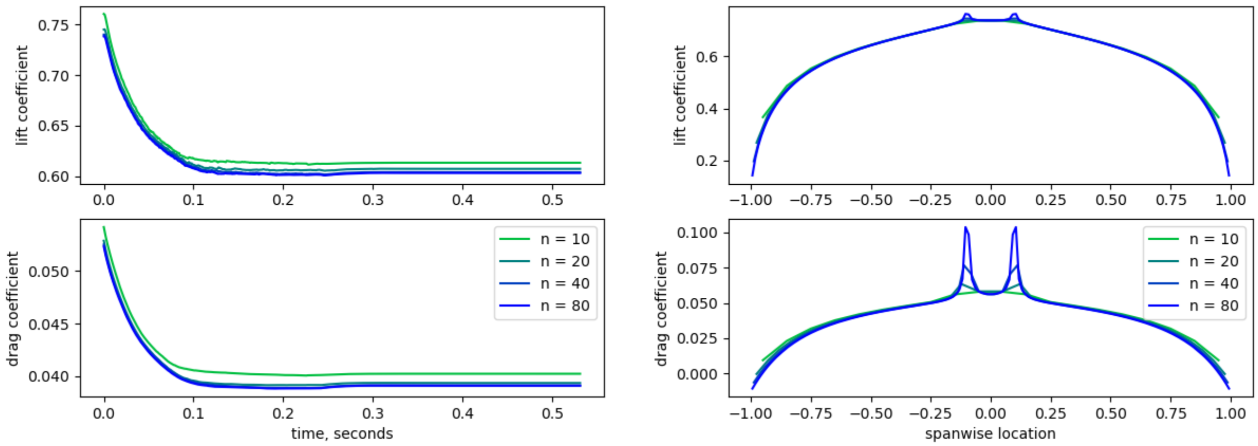

Fig. 6 Convergence testing of the number of control points n of the wing without rotors determines $n = 20$.

D. Rotor Influence on Dynamic Aeroelastic Response

It is also worth examining the aeroelastic response of the wing with and without rotors. We plot the tip displacement vs. time with and without rotors, and its frequency domain analysis, in Fig. 12. We note two things: first, the case with rotors appears to oscillate with higher frequency and amplitude than the case without rotors. Second, the frequencies present are much more spread for the rotors case, indicating that the rotor may be exciting other oscillatory modes. This suggests that including the unsteady rotor wake in the structural solver will result in higher bending stresses and greater fatigue than without.

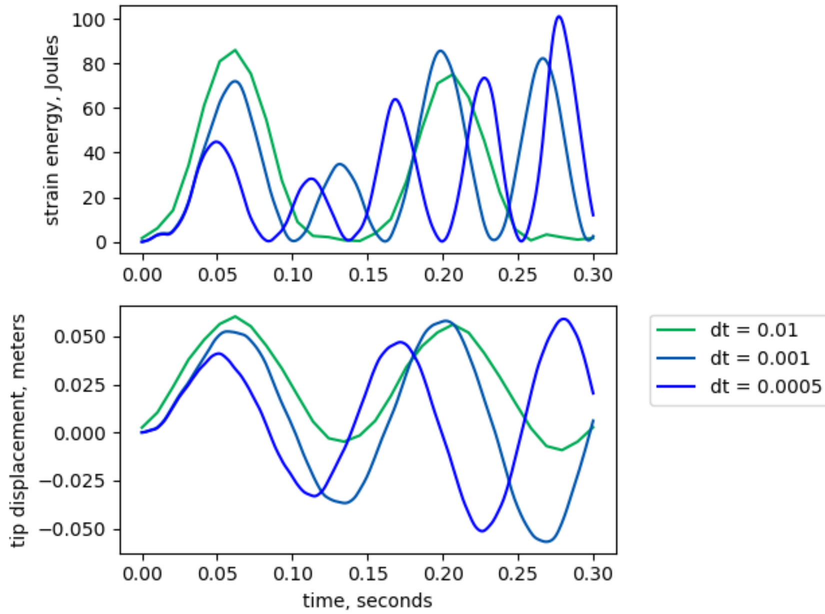

Fig. 7 Preliminary convergence testing of the timestep of the coupled solvers.

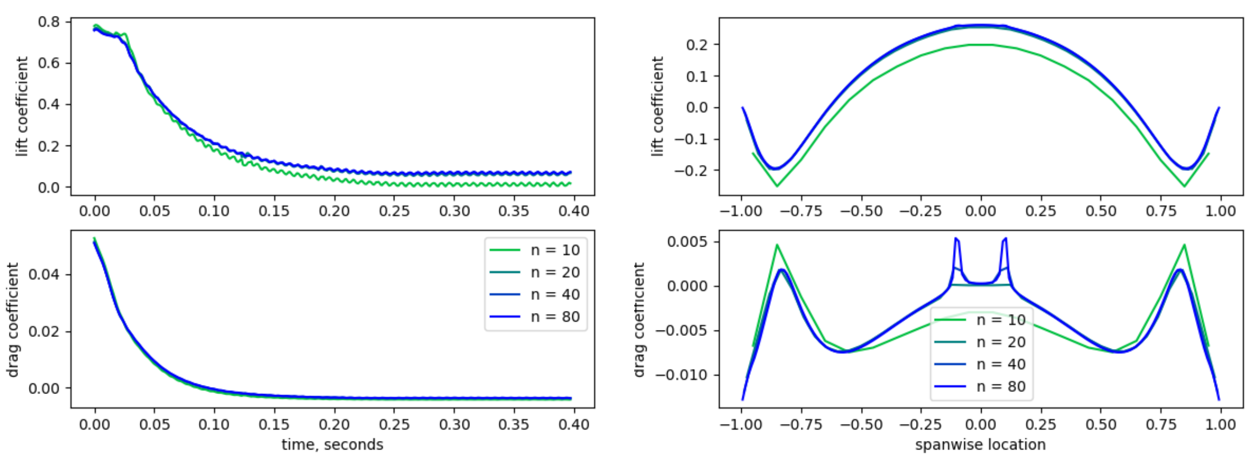

Fig. 8 Preliminary convergence testing of the number of control points *nr* of each rotor blade.

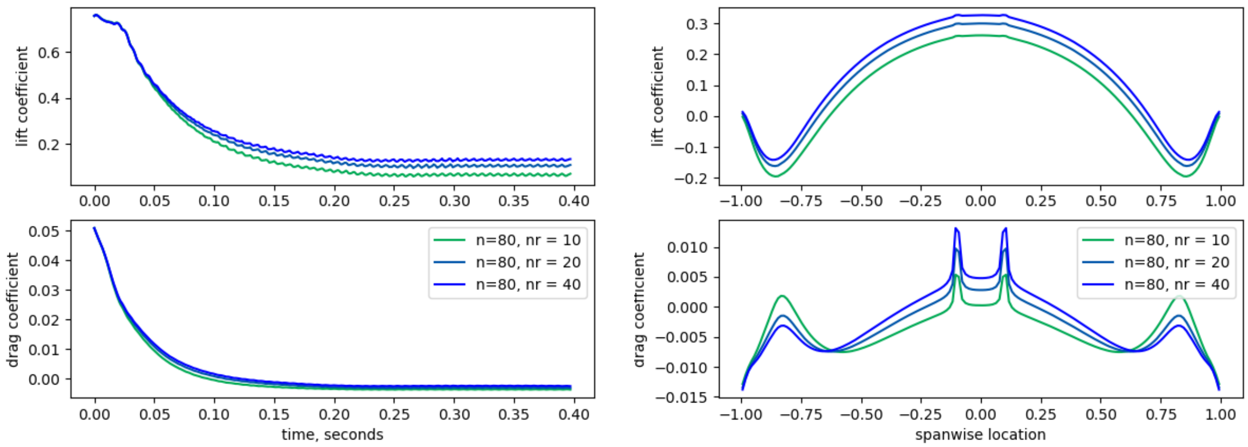

Fig. 9 Preliminary convergence testing of the number of control points nr **of each rotor blade.**

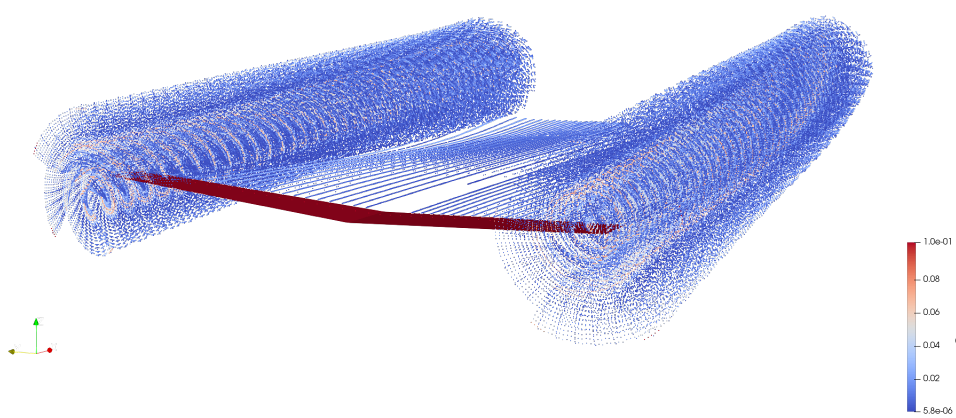

Fig. 10 Wake of the eCRM-002 without the structure solver. $n = 20$, $nr = 20$, **and** $\Delta t = 0.001$**.**

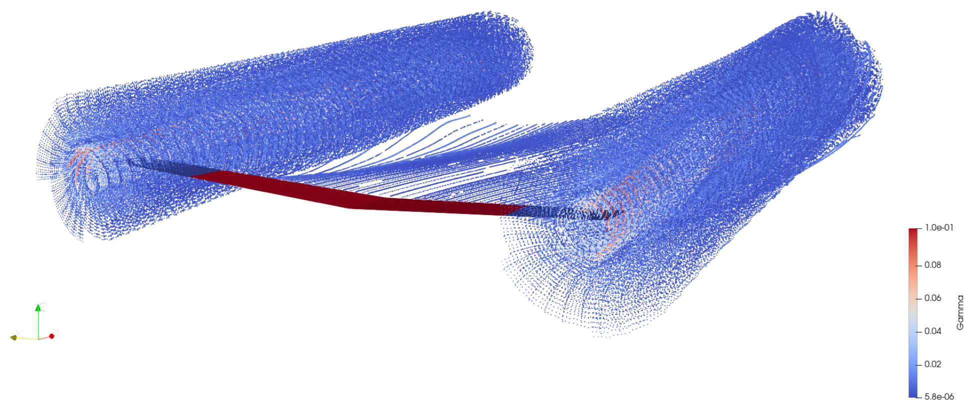

Fig. 11 Wake of the eCRM-002 with the structural solver. $n = 20$, $nr = 20$, **and** $\Delta t = 0.001$.

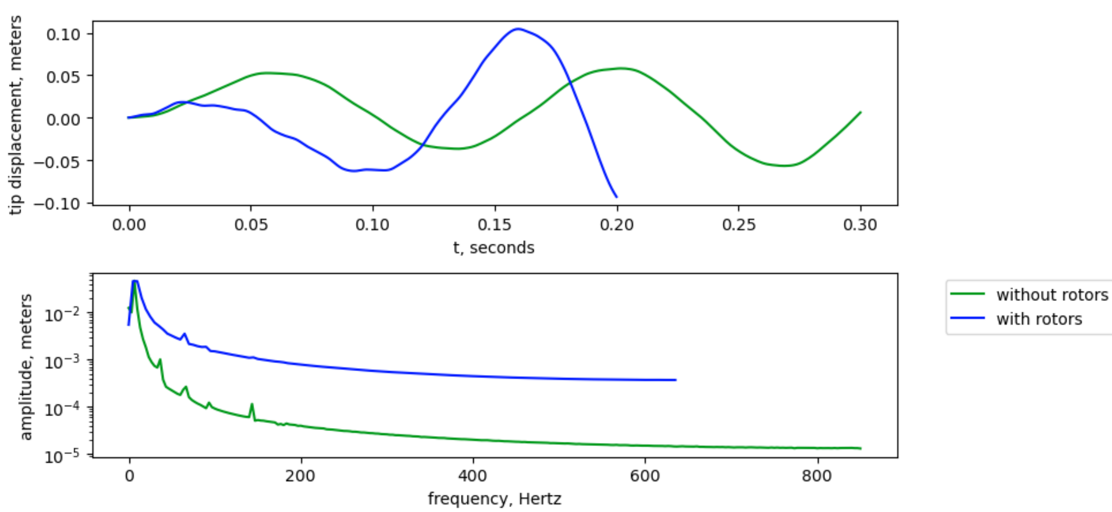

Fig. 12 Aeroelastic response of the wing with and without rotors.

IV. Conclusion

The present work introduces a framework for predicting aerostructural dynamics. We combine a Reissner-Mindlin shell theory for computing deflections and a viscous vortex particle for capturing wakes, perform preliminary convergence studies, and preliminary results for the eCRM-002 main wing. Interestingly, we notice more highly concentrated vorticity in the wingtip vortices. When comparing the performance with and without rotors, we notice greater amplitudes and a wider range of frequencies than without the rotor.

Acknowledgments

The material presented in this paper is based upon work supported by NASA under award No. 80NSSC21M0070.

References

[1] Sarojini, D., Duca, R., Solano, H. D., Chakraborty, I., Briceno, S. I., and Mavris, D. N., "Framework to assess effects of structural flexibility on dynamic loads developed in maneuvering aircraft," *2018 Aviation Technology, Integration, and Operations Conference*, 2018, p. 4147. https://doi.org/https://doi.org/10.2514/6.2018-4147.

[2] Veldhuis, L. L. M., "Review of Propeller-Wing Aerodynamic Interference," *24th International Congress of the Aeronautical Sciences*, 2004. URL http://icas.org/ICAS_ARCHIVE/ICAS2004/PAPERS/065.PDF.

[3] Montagnani, D., Tugnoli, M., Fonte, F., Zanotti, A., Syal, M., and Droandi, G., "Mid-Fidelity Analysis of Unsteady Interactional Aerodynamics of Complex VTOL Configurations," *45th European Rotorcraft Forum (ERF 2019)*, 2019, pp. 1–11.

[4] Witkowski, D. P., Lee, A. K., and Sullivan, J. P., "Aerodynamic interaction between propellers and wings," *Journal of Aircraft*, Vol. 26, No. 9, 1989, pp. 829–836. https://doi.org/10.2514/3.45848.

[5] Wilke, G., "Aerodynamic Performance of Two eVTOL Concepts," *Symposium der Deutsche Gesellschaft fur Luft-und Raumfahrt*, Springer, 2018, pp. 392–402.

[6] Reddinger, J.-P., McIntosh, K., Zhao, D., and Mishra, S., "Modeling and Trajectory Control of a Transitioning Quadrotor Biplane Tailsitter," 2019.

[7] Kim, H. D., Perry, A. T., and Ansell, P. J., "A review of distributed electric propulsion concepts for air vehicle technology," *2018 AIAA/IEEE Electric Aircraft Technologies Symposium (EATS)*, IEEE, 2018, pp. 1–21.

[8] Ye, L., Zhang, Y., Yang, S., Zhu, X., and Dong, J., "Numerical simulation of aerodynamic interaction for a tilt rotor aircraft in helicopter mode," *Chinese Journal of aeronautics*, Vol. 29, No. 4, 2016, pp. 843–854.

[9] Wu, Z., Li, C., and Cao, Y., "Numerical simulation of rotor–Wing transient interaction for a tiltrotor in the transition mode," *Mathematics*, Vol. 7, No. 2, 2019, p. 116.

[10] Moore, K., and Ning, A., "Takeoff and Performance Tradeoffs of Retrofit Distributed Electric Propulsion for Urban Transport," Ph.D. thesis, Brigham Young University, 2019. https://doi.org/10.2514/1.C035321, URL https://scholarsarchive.byu.edu/cgi/viewcontent.cgi?article=4204&context=facpub.

[11] Chauhan, S. S., and Martins, J., "RANS-based aerodynamic shape optimization of a wing considering propeller-wing interaction," *AIAA Scitech 2020 Forum*, 2020, p. 1764.

[12] Felker, F. F., and Light, J. S., "Rotor/wing aerodynamic interactions in hover," *Annual Forum of the American Helicopter Society*, 1986.

[13] Fratello, G., Favier, D., and Maresca, C., "Experimental and numerical study of the propeller/fixed wing interaction," *Journal of AIRCRAFT*, Vol. 28, No. 6, 1991, pp. 365–373.

[14] Young, L. A., and Derby, M. R., "Rotor/wing interactions in hover," *NASA TM*, Vol. 211392, 2002.

[15] Solano, D., Sarojini, D., Rajaram, D., and Mavris, D. N., "Adjoint-based analysis and optimization of beam-like structures subjected to dynamic loads," *Structural and Multidisciplinary Optimization*, Vol. 65, No. 2, 2022, pp. 1–19. https://doi.org/https://doi.org/10.1007/s00158-021-03141-5.

[16] Sarojini, D., and Mavris, D., "Structural Analysis and Optimization of Wings Subjected to Dynamic Loads," *AIAA Journal*, Vol. 60, No. 2, 2022, pp. 1013–1023. https://doi.org/https://doi.org/10.2514/1.J060931.

[17] Kjellgren, P., Sivasubramanian, J., Cerchie, D., Cullen, L., Hassan, A., and Wygnanski, I., "Download alleviation for the XV-15: computations and experiments of flows around the wing," *2002 Biennial International Powered Lift Conference and Exhibit*, 2002, p. 6007.

[18] Lee, H., and Lee, D.-J., "Numerical investigation of the aerodynamics and wake structures of horizontal axis wind turbines by using nonlinear vortex lattice method," *Renewable Energy*, Vol. 132, 2019, pp. 1121–1133.

[19] Alvarez, E., and Ning, A., "Modeling Multirotor Aerodynamic Interactions Through the Vortex Particle Method," *AIAA Aviation Forum*, 2019, p. 3191. https://doi.org/10.2514/6.2019-2827, URL https://scholarsarchive.byu.edu/facpubhttps://scholarsarchive.byu.edu/facpub/3191.

[20] Savino, A., Cocco, A., Zanotti, A., Tugnoli, M., Masarati, P., and Muscarello, V., "Coupling Mid-Fidelity Aerodynamics and Multibody Dynamics for the Aeroelastic Analysis of Rotary-Wing Vehicles," *Energies*, Vol. 14, No. 21, 2021, p. 6979.

[21] Kennedy, G. J., and Martins, J. R., "A parallel finite-element framework for large-scale gradient-based design optimization of high-performance structures," *Finite Elements in Analysis and Design*, Vol. 87, 2014, pp. 56–73. https://doi.org/10.1016/j.finel.2014.04.011.

[22] van Schie, S. P. C., Zhao, H., Jiayao, Y., Ru, X., Hwang, J. T., and Kamensky, D., "Solver-Independent Aeroelastic Coupling For Large-Scale Multidisciplinary Design Optimization," *AIAA Scitech 2023 Forum*, 2023.

[23] Ha, T. H., *System-level performance investigation of eVTOL concepts using large-scale DEP-focused design optimizations*, University of California, San Diego, 2020.

[24] Logg, A., Mardal, K.-A., Wells, G. N., et al., *Automated Solution of Differential Equations by the Finite Element Method*, Springer, 2012.

[25] Alvarez, E. J., Mehr, J., and Ning, A., "FLOWUnsteady: An Interactional Aerodynamics Solver for Multirotor Aircraft and Wind Energy," *AIAA AVIATION 2022 Forum*, 2022, p. 3218.

[26] Alvarez, E. J., "Reformulated Vortex Particle Method and Meshless Large Eddy Simulation of Multirotor Aircraft," 2022.

[27] Pedrizzetti, G., "Insight into singular vortex flows," *Fluid Dynamics Research*, Vol. 10, No. 2, 1992, p. 101.

[28] Campello, E. M. B., Pimenta, P., and Wriggers, P., "A triangular finite shell element based on a fully nonlinear shell formulation," *Computational Mechanics*, Vol. 31, 2003, pp. 505–518. https://doi.org/10.1007/s00466-003-0458-8.